Published in final edited form as:
J Neural Eng. 2015 February ; 12(1): 016017. doi:10.1088/1741-2560/12/1/016017.

Functional recordings from awake, behaving rodents through a microchannel based regenerative neural interface

Russell K. Gore[1,5], **Yoonsu Choi**[4,5], **Ravi Bellamkonda**[2], and **Arthur English**[3]

Russell K. Gore: rustygore@gmail.com; Arthur English: medae@emory.edu

[1]Department of Neurology, Emory University School of Medicine, 550 Peachtree Street NE, 9th Floor MOT, Atlanta, Georgia 30308

[2]Wallace H Coulter Department of Biomedical Engineering, Georgia Institute of Technology & Emory School of Medicine, 1760 Haygood Drive NE, Atlanta, Georgia 30322

[3]Department of Cell Biology, Emory University School of Medicine, 615 Michael Street, Room 405P Atlanta, Georgia 30322

[4]Department of Electrical Engineering, The University of Texas – Pan American, 1201 West University Drive, ENGR 3251, Edinburg, TX 78539

Abstract

Objective—Neural interface technologies could provide controlling connections between the nervous system and external technologies, such as limb prosthetics. The recording of efferent, motor potentials is a critical requirement for a peripheral neural interface, as these signals represent the user-generated neural output intended to drive external devices. Our objective was to evaluate structural and functional neural regeneration through a microchannel neural interface and to characterize potentials recorded from electrodes placed within the microchannels in awake and behaving animals.

Approach—Female rats were implanted with muscle EMG electrodes and, following unilateral sciatic nerve transection, the cut nerve was repaired either across a microchannel neural interface or with end-to-end surgical repair. During a 13-week recovery period, direct muscle responses to nerve stimulation proximal to the transection were monitored weekly. In two rats repaired with the neural interface, four wire electrodes were embedded in the microchannels and recordings were obtained within microchannels during proximal stimulation experiments and treadmill locomotion.

Main results—In these proof-of-principle experiments, we found that axons from cut nerves were capable of functional reinnervation of distal muscle targets, whether regenerating through a microchannel device or after direct end-to-end repair. Discrete stimulation-evoked and volitional potentials were recorded within interface microchannels in a small group of awake and behaving animals and their firing patterns correlated directly with intramuscular recordings during locomotion. Of 38 potentials extracted, 19 were identified as motor axons reinnervating tibialis anterior or soleus muscles using spike triggered averaging.

[5]Authors were equal contributors to this work.

Significance—These results are evidence for motor axon regeneration through microchannels and are the first report of *in vivo* recordings from regenerated motor axons within microchannels in a small group of awake and behaving animals. These unique findings provide preliminary evidence that efferent, volitional motor potentials can be recorded from the microchannel-based peripheral neural interface; a critical requirement for any neural interface intended to facilitate direct neural control of external technologies.

Keywords

Neural Interface; Nerve Regeneration; Neuroprosthesis; Nerve Injury; Peripheral Nerve; Microchannels

1. Introduction

To provide connections between the nervous system and external technologies, such as limb prosthetics, a neural interface is required. In amputees, such technologies could provide direct neural control of prosthetic movements as well as restore sensory feedback by functionally accessing damaged efferent motor and afferent sensory pathways. The peripheral nerve is one target for such bidirectional interfacing, with renewed interest generated by reports that peripheral neural tissue is viable for interfacing even years after injury or amputation (Dhillon, Lawrence et al. 2004). Interfacing directly with peripheral nerves has the advantage of minimizing surgical risk and complications associated with technologies such as cortical implants, avoiding the reactive gliosis and electrode failure which plagues cortical interface designs due to tethering forces and mechanical damage (Hariz 2002, Polikov, Tresco et al. 2005).

In order to facilitate highly selective recording and stimulation, current designs for peripheral nerve interfacing attempt to interface directly with peripheral axons(Rutten 2002). Less selective designs, such as cuff electrodes, provide selectivity only at the level of the peripheral nerve fascicle due to electrodes positioned outside the epineurium (Badia, Boretius et al. 2011). Designs affording direct contact with axons include penetrating electrodes, such as the longitudinal intrafascicular electrode (LIFE) and the Utah Slanted Electrode Array (USEA), and regenerative electrode designs, such as the sieve electrode and microchannel based neural interfaces (Mannard, Stein et al. 1974, Edell 1986, Akin, Najafi et al. 1994, Navarro, Calvet et al. 1998, Rutten 2002, Garde, Keefer et al. 2009, Serra, Bostock et al. 2010, FitzGerald, Lago et al. 2012, Minev, Chew et al. 2012, Clements, Mukhatyar et al. 2013).

The ability to record activity from individual axons through direct contact has been shown for some penetrating and regenerative interface designs. Penetrating electrodes consist of projections with exposed electrode sites designed to penetrate the intact nerve and contact axons directly within peripheral nerve fascicles. This method has been demonstrated in the rat sciatic nerve to allow stable recordings from axons either through chronic implantation or with acute recordings over time (Branner, Stein et al. 2004, Serra, Bostock et al. 2010). Although penetrating electrodes can provide selective, stable recordings from the peripheral nerve, the device has limited electrode sites and recordings can only be obtained from the limited number of nerve fascicles penetrated during implantation.

Regenerative electrodes consist of a conduit with embedded electrodes through which axons in a transected peripheral nerve are permitted to regenerate, resulting in direct contact between electrodes and regenerating axons. The sieve electrode, a flat wafer with multiple holes ringed with embedded electrodes, demonstrates highly selective stimulation after regeneration (Akin, Najafi et al. 1994, Navarro, Calvet et al. 1998, Ceballos, Valero-Cabre et al. 2002). However, recordings from sieve electrode sites is limited to high amplitude potentials and recordings depend on the proximity of electrodes to nodes of Ranvier (Rutten 2002, Lago, Ceballos et al. 2005, Castro, Negredo et al. 2008). Sieve electrode designs also limit nerve regeneration demonstrated by poor distal axon counts and neuroma formation(Klinge, Vafa et al. 2001, Lago, Ceballos et al. 2005, Castro, Negredo et al. 2008). Poor distal regeneration is likely influenced by channel size with *in vivo* experiments suggesting that fasciculation of the regenerating nerve blocks ingrowth of axons in smaller caliber channels(Zhao, Drott et al. 1997, Rutten 2002, FitzGerald, Lago et al. 2012, Srinivasan, Tahilramani et al. in press). In addition axon ingrowth and regeneration appear to be influence by device transparency, defined as the open surface area available for axons to regenerate. Increasing transparency, by minimizing structural obstruction of regeneration by the device scaffold, improves axon ingrowth and distal regeneration(Lago, Ceballos et al. 2005, Ramachandran, Schuettler et al. 2006, Lacour, Atta et al. 2008, Garde, Keefer et al. 2009, FitzGerald, Lago et al. 2012).

An effective regenerative neural interface design should both promote regeneration into the device to contact electrodes and be capable of recording from small populations of regenerated axons. In order to facilitate highly selective recordings, recent regenerative designs have incorporated microchannels through which axons regenerate and directly contact embedded electrodes (FitzGerald, Lacour et al. 2009, Wieringa, Wiertz et al. 2010, FitzGerald, Lago et al. 2012, Srinivasan, Tahilramani et al. in press). A principle challenge in peripheral neural interfacing is the detection of small amplitude peripheral neural signals amid much larger muscle signals. Microchannel technology is demonstrated to amplify small potentials by increasing extracellular resistance within the insulated microchannel and improve recordings in myelinated axons with microchannel lengths designed to ensure at least one Node of Ranvier is present (FitzGerald, Lacour et al. 2009). The amplification of microchannel potentials improves *in vitro* within smaller microchannels where limiting extracellular volume further increases extracellular resistance. Smaller microchannels may also improve recording and stimulating selectivity by mechanically separating regenerating axons(Wieringa, Wiertz et al. 2010). However, leveraging the amplifying properties of microchannels must also be balanced with design characteristics to optimize axon ingrowth and regeneration into microchannels. Although *in vitro* results disagree on the optimal microchannel caliber to promote sustained axon ingrowth, *in vivo* experiments, demonstrating fibrous sheath micro-fascicular formation within microchannels, and our own laboratory experience suggest that larger microchannels and increased device transparency are necessary to promote and support regeneration(Lacour, Atta et al. 2008, Wieringa, Wiertz et al. 2010, Srinivasan, Guo et al. 2011, FitzGerald, Lago et al. 2012, Srinivasan, Tahilramani et al. in press).

The recording of efferent, motor potentials is a critical requirement for a peripheral neural interface as these signals represent the user generated neural output intended to drive external devices such as a prosthetic limb. To date, regenerative neural interface designs have been demonstrated in experiments to record only stimulation evoked efferent potentials and sensory evoked afferent potentials in anesthetized animals (FitzGerald, Lago et al. 2012, Minev, Chew et al. 2012). In stimulation evoked experiments, proximal electrical stimulation evokes an action potential in the peripheral nerve that is recorded distally in axons regenerated within the device. Such responses are sampled from a mixed population of both efferent and afferent axons (motor and sensory axons), both evoked by proximal stimulation. These recordings do not represent volitional efferent axon signals generated by the user to drive motor output. Additionally, these experiments are conducted in anesthetized animals with surgical exposure of the sciatic nerve, an effective means with which to minimize concurrent muscle noise. Translation of peripheral neural interface technology into humans will require that these potentials are detectable in awake and behaving subjects (Stieglitz 2007). In order to demonstrate the detection of these efferent potentials, methods are required to time lock neural recordings with motor output in awake and behaving animals.

The goals of this study were to evaluate structural and functional neural regeneration through a microchannel neural interface and to characterize potentials recorded from electrodes placed within the microchannels in awake and behaving animals. We show in these proof-of-principle experiments that axons of cut nerves are capable of functional reinnervation of distal muscle targets similarly in both the microchannel device and direct repair groups. In addition, in a small group of awake and behaving animals our preliminary results demonstrate discrete stimulation-evoked and volitional potentials recorded within interface microchannels. The firing patterns of these potentials correlated directly with intramuscular EMG recordings during locomotion, suggesting that we are recording from groups of motor axons regenerated within microchannels.

2. Methods

Subjects were eighteen female Lewis rats (∼ 250g). All procedures conformed to the Guide for the Care and Use of Laboratory Animals of the Institute of Laboratory Animal Resources, Commission on Life Sciences, National Research Council (National Academy Press, Washington, DC, 1996). They were reviewed and approved by the Institutional Animal Care and Use Committee of Emory University. Methods for construction of the chronic nerve stimulating cuff, chronic muscle electrode implantation, EMG recordings in freely moving rats, M-response and H-reflex elicitation, and sciatic nerve transection and repair were similar to those previously described in detail (Chen and Wolpaw 1995, English 2005, Sabatier, Redmon et al. 2008, Sabatier, Bao et al. 2011) and are summarized here. Additional procedures for fabrication and implantation of the regenerative neural interface and microchannel recordings are described in detail. Some of the control data from animals in the Control group (n=6) have been reported previously (Boeltz, Ireland et al. 2013).

2.1. Neural Interface Fabrication

The neural interface is illustrated schematically in Figure 2(A) and shown just prior to implantation in Figure 2(B) and (C). The design consisted of a microchannel scaffold with integrated microwire electrodes. A PDMS micro-molding technique was used to fabricate 3 mm long microchannel scaffolds. Polysulfone tubes with a 1.5mm inner diameter were used as PDMS casting molds into which commercially available microwires were inserted and used as microchannel molding materials. The 1.5mm diameter mold was used as an approximation of the diameter of the rat's sciatic nerve. Both 200 μm and 75 μm diameter microchannels were incorporated into the scaffold with 17 and 65 microchannels of each diameter, respectively. Microchannel diameters were selected to maximize extracellular resistance without impeding axon regeneration (75 μm) and allow for the integration of microchannel electrodes, within the larger microchannels, without impeding axon regeneration (200 μm). After mixing and degassing PDMS (Sylgard 184, Dow), a bundle of microwires was inserted into a polysulfone tube which was filled with PDMS using a syringe. The PDMS was cross-linked in a convection oven at 100°C for 2 hours and the polysulfone tube was removed using a fine knife. The remaining construct was soaked in chloroform to swell the PDMS and loosened contact with the imbedded microwire molds. The microwires were then pulled out of the cross-linked PDMS structure forming the microchannels within the scaffold. The structure was then transferred from chloroform to 70% ethanol in order to shrink the PDMS and rinsed with DI water.

In order to integrate recording electrodes, 75 μm thick single core microwires (50 μm metal, 25 μm insulation, Stablohm 800A, California fine wire) were inserted into four of the 200 μm microchannels. These dimensions allowed for adequate cross-sectional microchannel space to optimize axonal regeneration through PDMS based microchannel scaffolds (FitzGerald, Lacour et al. 2009). Recording electrodes consisted of commercially available insulated fine microwire. The insulation was retained on all but the cut end of each integrated microwire, meaning that only the 75 μm diameter cross section of the tip was exposed. Integrated microwires were inserted into the distal end of the scaffold and curved to avoid obstructing any axons regenerating out of the distal end of the scaffold. The microwire tip with exposed recording surface was embedded into the center of the length of the microchannel in order to sample potentials amplified from within the microchannel construct. Microchannel potentials were recorded using a configuration illustrated schematically in Figure 2(A & B) with the ground electrode positioned within the polysulfone suture guide at the distal end of the device. These insulated wires were then directed along the outside of the scaffold and secured using medical grade UV glue (1187-M-SV01, DYMAX). Polysulfon suture guides were fitted around the ends of the neural interface prior to implantation to facilitate alignment and attachment of the transected proximal and distal nerve stumps and guide regenerating axons from the proximal nerve stump into the scaffold microchannels and from the microchannels into the original distal nerve segment.

2.2. Muscle electrode implantation, sciatic nerve transection, and neural interface implantation

Each rat was implanted under general anesthesia with sodium pentobarbital [60 mg/kg] administered intraperitoneally and supplemented as needed. All surgical procedures were performed under aseptic conditions. The experimental design for the study is shown in Figure 1. To record muscle (EMG) activity, pairs of multi-stranded stainless steel fine-wire electrodes (Cooner Wire Co, Chatsworth CA) were stripped of their final 0.5 mm of Teflon insulation and implanted into the right soleus (SOL) (eight rats) or the right SOL and right tibialis anterior (TA) (ten rats) muscles. To record responses from SOL and TA evoked from nerve stimulation, a bipolar stimulating nerve cuff-type electrode made of silicone rubber containing a pair of electrodes made from the same fine-wire was placed on the right proximal sciatic nerve (prior to the bifurcation of the tibial and common fibular nerves) (Stein, Nichols et al. 1977). In all animals wires from the muscle electrodes, the nerve cuff, and the neural interface were passed subcutaneously to small, 1cm diameter, head stage connectors (Plastics One, Roanoke, VA) secured to the skull with stainless steel screws and dental cement.

In sixteen of the eighteen experimental rats, muscle electrodes were first implanted and evoked EMG activity was recorded from SOL in intact animals for 14-24 days before nerve transection and neural interface implantation or end-to-end repair. In two rats with microchannel electrodes incorporated into the neural interface the sciatic nerve was transected and the interface surgically implanted as described above at the time of muscle electrode implantation. In these animals initial evoked EMG activity was recorded immediately after muscle and cuff implantation, prior to nerve transection, in anesthetized animals. In all rats, the sciatic nerve was exposed distal to the sciatic stimulation cuff (proximal to the branching of the sural nerve) and cut completely with sharp scissors. In the Microchannel group (n=10) the proximal and distal stumps were immediately aligned with the proximal and distal ends of the neural interface integrated polysulfone suture guide. The nerve stumps were inserted approximately 1.5mm into the suture guide, flush with the neural interface, to encourage axon regeneration into microchannels and to minimize regeneration outside of the neural interface. The nerve stumps were then secured using 10-0 suture. In the Control group (n=8) the proximal and distal stumps were immediately aligned and reattached with fibrin glue as previously described (Boeltz, Ireland et al. 2013). Postoperatively, animals were placed under a heating lamp and given an analgesic (oral buprenorphine). Over the course of the experiment animal well-being was carefully monitored daily. Laboratory lights were dimmed from 9:00 P.M. to 6:00 A.M. each day.

2.3. Nerve conduction studies

Electrophysiological data collection resumed after a 20 day recovery period following transection and continued once weekly for ~90 days. During recording sessions the head mounted connector was attached to a 40cm long flexible, metal-jacketed cable allowing the animal to move freely in the cage or on the treadmill during locomotion experiments. The cable conveyed the wires from the stimulation cuff, muscle electrodes, and microchannel electrodes to an amplifier (EMG gain 1k, bandwidth 100-1,000 Hz; Microchannel electrode (ENG) gain 10k, bandwidth 1-10 kHz) and a stimulus isolation unit. The higher frequency

bandwidth used for recording ENG potentials was employed to minimize the contribution of any passively conducted EMG potentials to our recordings from microchannels. The power spectrum for EMG potentials is maximal at lower frequencies and will be attenuated approximately 18 dB by our filters (Basmajian and DeLuca 1985). Stimulus delivery and data collection were under the control of a computer system, which monitored ongoing EMG activity (filtered at 100–1000 Hz, sampled at 10,000 Hz) from SOL and TA muscles continuously for the recording session. Whenever the absolute value (equivalent to the full wave rectified value) of background EMG activity remained within defined range for a 100 ms period, the computer initiated a trial and a very short (0.1 ms) monophasic stimulus pulse was delivered to the sciatic nerve via the implanted cuff electrode. There was a minimum of 3 s inter-stimulus delay, previously demonstrated by this laboratory to result in consistent EMG responses without muscle fatigue (English, Chen et al. 2007). In each trial, the computer stored the 50 ms of activity from implanted electrodes prior to stimulation (i.e., the background interval), delivered the stimulus pulse to the sciatic nerve cuff, and stored the EMG or microchannel electrode activity for another 100 ms. During the period after nerve transection and before the muscle reinnervation, the stimulus was increased to a maximum of 2.5 times the average pre-transection pulse amplitude or to the level evoking the target M-response amplitude, whichever was lower.

In intact animals two compound muscle action potential responses were elicited in response to sciatic nerve stimulation: an initial direct muscle response (M-response); and a longer latency H reflex. The H reflex is the result of afferent axon stimulation with resulting synaptic activation of motoneurons. The SOL responses to sciatic cuff stimulation were displayed in a raster format to determine the latency window of the initial (M-response) and latent (H reflex) waveforms (typically 6–10 ms after the initial response). The amplitudes of the two evoked responses were defined as the average rectified voltage within user-defined latency windows after cuff stimulation. In intact rats, these windows were 0.5-4 msec and 5-11 msec for the M response and H reflex, respectively (Chen and Wolpaw 1995). After nerve transection and axon regeneration, both the latency and duration were longer (English, Chen et al. 2007). In each experimental trial, a ramp of successively increasing stimulus voltages, ranging from sub-threshold to supra-maximal, was applied to generate full M-response, H-reflex, and Microchannel recruitment curves. The incremental increase in stimulation voltage during the ramp was calculated to include a minimum of 100 stimulations ranging from sub-threshold (0.1mV) to supra-maximal (1.5 times the average pre-transection pulse amplitude). Final evoked responses for each animal at each recording session were averages of multiple stimulus trials, corrected for background EMG activity.

The maximum M response (Mmax) and the maximum H reflex (Hmax) amplitudes were measured separately during each recording session. The M-response and H reflex latency also were measured, defined as the time from stimulus application to the initiation of the measured response. Each of these measured parameters were expressed as a percentage of the corresponding average peak amplitudes and average latencies obtained in pre-transection recordings. Values of both Mmax and Hmax during the post-injury study period were fit with a least squares linear regression method. Significance of differences in slopes between Microchannel and Control groups were made using multiple linear regression analysis (Statistica, StatSoft).

2.4. Locomotor EMG activity and microchannel recordings

Activity in SOL, TA, and microchannels was recorded during treadmill locomotion from the implanted EMG and microchannel electrodes at 7, 9, and 10 wks after nerve transection and neural interface implantation in a small group of animals (n=2). Details of locomotion recording conditions and procedures are detailed in our laboratory's previous publications (Sabatier, Redmon et al. 2008, Sabatier, Bao et al. 2011). Muscle activity and video records were synchronized to an LED pulse in the video field whose timing was recorded simultaneously with EMG and microchannel activity. Following recorded locomotion sessions, videos of the selected step cycles were subjected to single-frame analysis. During step cycles in which rats walked at constant speed on the treadmill, the timing of paw contact and paw off was determined and used to extract the EMG and microchannel activity during individual step cycles. *Post hoc* analysis of EMG and microchannel activity was performed offline using custom unit extraction and spike triggered averaging software (LabVIEW, National Instruments, 2011). Waveforms were sorted and averaged offline to isolate individual potentials. Spike triggered averaging was used to analyze individual potentials firing patterns and correlated directly with intramuscular recordings. During *post hoc* analysis, microchannel potentials were correlated with distal muscle potentials. Microchannel potentials were labeled as motor potentials if the peak of the recorded distal muscle potential occurred later than the peak of the triggering microchannel potential recorded in the device.

2.5. Histology

After electrophysiology experiments, animals were euthanized with an overdose of sodium pentobarbital (ip) and perfused through the heart with saline followed by 4% paraformaldehyde. The integrity of the EMG electrodes, nerve cuff, and neural interface were examined and the regenerated sciatic nerve and the intact neural interface were explanted and post-fixed for 24 hours in 4% paraformaldehyde (Sigma-Aldrich). The samples were rinsed again in PBS and transferred to 30% sucrose solution in phosphate buffer, pH 7.4, for cryoprotection. The samples were then embedded in O.C.T. gel (Tissue Tek) and stored at -40°C until the time of cryosectioning. A cryostat (CM30505, Leica) was used to collect 100 μm thick cross sections. Sections were later reacted for immunofluorescent demonstration of markers on axons (NF160, 1:500 dilution, Sigma–Aldrich) and Schwann cells (S100, 1:250, Dako). Nuclei were labeled with DAPI (Invitrogen) in PBS at a concentration of 10 mM. The following secondary antibodies were used: Goat anti-rabbit IgG Alexa 488/594, goat anti-mouse IgG1 Alexa 488/594. Immunohistochemistry was conducted as previously described (Clements, Mukhatyar et al. 2013). Briefly, sections were first incubated for one hour at room temperature in a blocking solution of 4% goat serum (Gibco) in PBS containing 0.5% Triton X-100 (Sigma). Sections were then incubated overnight at 4 °C in a mixture of primary antibody and blocking solution, then washed and incubated once more for 1 h at room temperature in a solution of secondary antibody, diluted 1:220 in 0.5% Triton in PBS. This incubation was followed by a 10-min incubation in DAPI solution. Finally, the sections were washed once more, dried, and cover-slipped for evaluation. Sections were imaged using a confocal microscope (Zeiss LSM 700).

3. Results

3.1 Microchannel interface fabrication

A microchannel interface was developed and fabricated using a flexible, biocompatible polyimide substrate (PDMS) and commercially available microwire. The fabrication technique allows for customizable microchannel geometry including device length, the number of incorporated microchannels, and microchannel diameter. Histology results indicate that tissue regenerated within microchannels and confirm the presence of axons and Schwann cells within both microchannel diameters.

3.2 Functional reinnervation in Microchannel vs. Control groups

Nerve conduction studies were performed weekly following a 20-day recovery period with regeneration through the microchannel neural interface to evaluate the extent of functional reinnervation of distal muscle targets. At each recording session, the sciatic nerve was stimulated through the implanted cuff electrode proximal to the implanted device. Stimuli were delivered over a broad range of intensities, ranging from subthreshold to supramaximal to insure that the maximal evoked responses were detected. Representative rectified and averaged soleus EMG muscle responses to sciatic stimulation recorded from a single rat prior to and at different time points following transection and repair through the microchannel neural interface are shown in Figure 3(A). During the first 2-3 weeks following nerve transection there is no response in the denervated muscle. Over time, with progressive muscle reinnervation and myelination through the microchannel neural interface, restoration of M and H responses to pre-transection amplitude and latency is observed. Restored direct muscle responses whose amplitudes were small but significantly greater than the pre-stimulus background EMG activity were observed within 30 days after sciatic transection in all animals. Over time the amplitude of the direct muscle response (M), the H reflex response (H), and the response latency were restored to near baseline values (Fig. 3). Stimulation evoked both direct M and H reflex responses prior to nerve transection (Intact) are illustrated.

The average direct muscle response (Mmax) and H reflex response (Hmax) amplitudes increased linearly during the study period in both Microchannel (n=10) and Control (n=6) groups as shown in Figures 3(B) and 3(C), respectively. Values for each response in both groups are expressed as a proportion of pre-transection recordings and are noted to increase over time approaching the horizontal dotted line, representing pre-transection values (1.0). These data were fitted to a least squares regression line and subjected to a multiple linear regression analysis. In this analysis the independent variables were survival time, experimental group (Microchannel=1 or Control=0), and their product, and the dependent variable was maximal evoked M amplitude or H reflex amplitude. In all cases the correlation coefficients were significant, suggesting that the linear model used was a good fit to the data; the slope of each line is significantly different from zero, meaning that both direct muscle response amplitudes (Mmax) and H reflex amplitudes (Hmax) in both the Microchannel and Control groups increase significantly over time. The slopes of these lines do not differ between groups for both Mmax amplitude ($p=0.06$) and Hmax amplitude ($p=0.43$). Thus, the time course of the restoration of the amplitude of both the M response

and H reflex during reinnervation after sciatic nerve section and repair with the microchannel device is not significantly different from that observed with direct repair of the cut nerve.

The average latency from stimulation to the direct muscle response decreased over time in both Microchannel and Control groups, returning to intact, pre-transection values as shown in Figure 3(D). Again values are expressed as a proportion of the same latency recorded prior to nerve transection. Latencies of these responses were restored nearly to pre-injury values by 80 days in both groups.

3.3 Neural regeneration within microchannels

Peripheral neural regeneration within microchannels was evaluated using confocal microscopy and an immunohistofluorescence assay to label axons and Schwann cells. Representative cross-sections of the neural interface explanted after nerve transection are illustrated in Figure 4. Figure 4(A) is a bright field microscopy image of the proximal scaffold 32 days after nerve transection, demonstrating regenerated tissue within microchannels (e.g. white arrows). Figure 4(B) is an image of a horizontal section of the distal neural interface. In it, axons immunoreactive for neurofilament proteins (NF-160, red) are seen within distal microchannels and exiting the microchannels to join the original distal nerve segment within the suture guide. In Figure 4(C) and 4(D) both 200 μm and 75 μm microchannels are illustrated. The central portion of both microchannels contains tissue with significant immunoreactivity to neurofilament proteins (NF-160, red) and Schwann cells (S-100, green) indicating that axons and Schwann cells regenerated into the microchannels. At higher magnification, axons were surrounded by Schwann cells in microchannels of both sizes, confirming the presence of axons in close proximity to myelinating Schwann cells.

During histologic analysis we encountered technical problems, which limited our ability to evaluate axon regeneration within microchannels systematically. Due to the material mismatch between hardened resin, the PDMS scaffold, and the regenerated tissue within microchannels we were not able to section the explanted PDMS scaffold into thin sections optimal for quantitative immunohistochemistry. There are reports describing the successful sectioning of PDMS microchannel scaffolds into 30-35 μm sections for histological analysis(Stoyanova, van Wezel et al. 2013). We were able to obtain much thicker frozen sections through the scaffold that were used for confocal microscopy and we were able to make thin sections from the immediate distal end of the device where regenerated tissue exited microchannels. From these sections, we identified tissues within device microchannels, using confocal microscopy, and axons and Schwann cells exiting microchannels (Fig. 4), in devices explanted after 32 days. A quantitative analysis of axons within microchannels was not attempted due to the sectioning difficulty noted. Thus, the histology results presented here are intended only to confirm that axons and Schwann cells regenerated into microchannels.

3.4 Electrical stimulation evoked microchannel recordings

Graded electrical stimulation applied to the sciatic cuff at survival times after axon regeneration evoked unique potentials recorded both in microchannels and in reinnervated

muscles. Among the small number of animals implanted with neural interfaces containing microchannel electrodes (n=2), potentials were recorded from all implanted microchannels containing imbedded electrodes (8/8 microchannel electrodes). Potentials with unique stimulation thresholds, latencies, and waveforms were recorded in different microchannels, suggesting the simultaneous recording of potentials from different axon populations in these awake and behaving animals (Figure 5). Examples of the amplitudes of evoked responses recorded simultaneously from two microchannel electrodes and an intramuscular EMG electrode (TA) during ramped sciatic cuff stimulation at 54 days after nerve transection are shown in Figure 5(A). Evoked EMG activity in TA (red) was first observed at stimulus strength of ∼1.0 V. At higher stimulus intensities, more motor units in TA were recruited until reaching maximal amplitude (Mmax) at ∼1.2 V, as shown by the raster of potentials of TA in Figure 5(C). Microchannel recruitment curves were a similar shape, while differing from one another and the TA EMG response in subtle ways. It is likely that at maximal stimulation intensities, the microchannel potentials recorded may represent both potentials evoked from regenerated axons in those microchannels but also contamination from much larger muscle potentials.

In recordings made at sub-maximal stimulation strengths we noted a recruitment of unique microchannel potentials in the absence of any TA EMG response. Sub-maximal stimulation response amplitudes are expanded in Figure 5(B) illustrating low amplitude thresholds in microchannels and consistent amplitude in the TA EMG response. In this example, the amplitude of TA EMG activity evoked from sciatic nerve stimulation remained constant over a wide range of intensities and was not significantly different from the background EMG activity recorded just prior to stimulation. Raster plots of microchannel and TA responses with unique microchannel potentials and waveforms recruited during progressive stimulation are illustrated in Figure 5(C). The response amplitudes of microchannel potentials increase to above background levels at stimulus intensities well below that for evoking TA EMG activity. At these sub-maximal stimulation strengths microchannel potentials were unique to individual microchannels, were unique waveforms, and amplitudes were smaller than the TA EMG background recorded, suggesting that these are recordings from either single axons or small populations of axons regenerated within microchannels. The microchannel 4 potential amplitude was noted to increase at ∼0.36 V and the corresponding waveform in the raster plot (sweep 4) was a short latency potential with triphasic morphology. During additional stimulations this potential was consistently present but changes in morphology and additional waveforms were recruited with different latencies (sweep 7). The microchannel 2 potential amplitude was noted to increase at ∼0.52 V corresponding to a waveform in the raster plot which is a longer latency (>4 ms) polyphasic potential likely originating from a slower conducting population of regenerated axons. These waveforms are noted to be unique between microchannels.

3.5. Locomotion Recordings

During treadmill locomotion, recordings were obtained from microchannels from which motor potentials were extracted and discriminated. Microchannel potentials with similar waveforms were identified in the locomotion recordings and extracted using a time-amplitude window discriminator routine. A total of 38 unique microchannel potentials were

extracted with amplitudes ranging from 37-194 μV (mean, 64.1 μV). All potentials were extracted from microchannels implanted in a small group of animals (n=2) in which distal muscle recordings could be correlated. We used spike triggered averaging to correlate these microchannel potentials with distal muscle activation and evaluate whether these potentials were from motor axons. Extracted microchannel potentials were used to trigger a signal averaging routine to extract time-locked replicates of muscle potentials from recordings made from TA and Soleus EMG electrodes and any temporally correlated ENG potentials from other microchannels (Figure 6A). Using these methods 17 microchannel potentials correlated only with TA activation (44.7%), two microchannel potentials correlated only with Soleus activation (5.3%), and 19 microchannel potentials did not correlate with either TA or SOL activation (50%). One microchannel potential correlating with TA EMG activity is illustrated in Figure 6(A) (inset). A robust response was found in the TA but not Soleus EMG activity (142 sweeps), and the peak of this extracted potential occurred at a very short latency (ca. 0.8 ms) *after* the peak of the triggering spike recorded in the microchannel, as illustrated by the vertical dashed line. No similar time-locked potentials were found in the other microchannels. We concluded that this extracted microchannel potential was from a motor axon or small group of motor axons that had reinnervated the TA muscle.

The firing patterns of these extracted motor axon potentials were evaluated during the step cycle. The timing of extracted potential activity was synchronized with video recordings of locomotion. The pattern of activity of the motor axon potential in Figure 6(A) (spike) is displayed with the raw activity in microchannel 2 (μCh2) and TA EMG activity for four consecutive step cycles during locomotion (Figure 6(B)). The shaded areas represent the swing phase and underlined time periods represent the stance phase of the step cycle. The motor axon spikes and microchannel 2 activity are noted to increase late in the swing phase with some corresponding activity in the TA muscle. Locomotor EMG activity in the reinnervated TA muscle is more prolonged than found in intact rats, consistent with previous reports from this laboratory (Sabatier et al 2011). The probability (p) of firing of this motor axon potential during a step cycle is greatest during the late swing phase (Figure 6(B), inset).

4. Discussion

Peripheral neural interfaces could provide stable access to central neural connections with the peripheral nerve without the need for implanted cortical ensembles. Regenerative neural interfaces are a promising technology to achieve this goal. Experiments were performed to evaluate the regeneration of motor axons through a microchannel neural interface and record from motor axons regenerated within microchannels in awake and behaving animals. Here we demonstrate motor axon regeneration through microchannels with restored motor responses consistent with end-to-end repair controls. In addition, these preliminary results represent the first report of *in vivo* recordings of regenerated motor axons within microchannels in a small group of awake and behaving animals, correlated directly with intramuscular recordings during locomotion. These unique preliminary findings suggest that volitional motor axon potentials can be recorded from our microchannel based peripheral neural interface; a critical requirement for any neural interface intended to facilitate direct neural control of external technologies.

4.1 Microchannel interface fabrication

Material substrates made from PDMS are commonly used in neural interface designs (Stieglitz, Beutel et al. 1997, FitzGerald, Lacour et al. 2009, Lacour, Benmerah et al. 2010). The present neural interface was implanted and recordings obtained for ∼90 days after nerve transection. In contrast to other reported microchannel-based peripheral interface designs, the neural interface fabrication technique presented here requires only commercially available materials and can be accomplished in most laboratories without the need for specialized equipment or clean room facilities (Lacour, Benmerah et al. 2010, Minev, Chew et al. 2012). A principle strength of this facile design is the accessibility of these techniques for investigators interested in peripheral neural interfacing or peripheral nerve injury and repair physiology. This technique also compliments other reported microneurography methods allowing for *in vivo* intraneural recordings of peripheral nerves during or after peripheral axon regeneration (Serra, Bostock et al. 2010).

In view of our present results, some modifications may be suggested in our neural interface design. In the present design the microchannel caliber and transparency resulted in adequate regeneration to promote active contact between axons and imbedded electrodes. These design considerations are discussed further below. In order to improve on these results novel electrode designs are needed to record within microchannels without impeding axon regeneration and to permit recording from multiple contacts within each microchannel. This would permit a direct comparison between recording paradigms and electrode configurations to optimize recording selectivity. In addition, additional headstage channels are necessary to simultaneously sample from larger numbers of microchannels and distal muscles. One of the principle strengths of our device design is it's simplicity and ease of fabrication so we are interested in exploring these simple designs compared with designs requiring much more advanced fabrication techniques to strike a balance between design performance and complexity (Srinivasan, Guo et al. 2011, FitzGerald, Lago et al. 2012, Minev, Chew et al. 2012, Srinivasan, Tahilramani et al. in press).

4.2 Motor axons regenerate through microchannels and restore distal functional connections

Following nerve transection, peripheral nerve regeneration and restoration of distal muscle function was demonstrated through the implanted microchannel neural interface. The restoration of motor function through the microchannel neural interface was consistent with previous results in end-to-end repair animals with progressive recovery of a distinct short latency response (M response) and long latency response (H reflex) (English, Chen et al. 2007). This result represents an improvement over similar *in vivo* experiments with the sieve electrode which demonstrated maximal muscle response amplitudes significantly below normal values even 7 months after implantation (Ramachandran, Schuettler et al. 2006). During the study period, regenerating motor axons elongated through microchannels and restored a substantial number of motor units. Such successful regeneration may be a function of the flexible material properties of PDMS and PDMS scaffold design characteristics such as channel diameter and device transparency; design features suggested for modification to improve regeneration based on experiments with the sieve electrode

(Lago, Ceballos et al. 2005, Ramachandran, Schuettler et al. 2006, FitzGerald, Lago et al. 2012).

In the present neural interface design, microchannel diameters were set at 75 μm or greater, as similar sieve and microchannel conduit diameters have improved myelinated axon regeneration compared with smaller diameters (Zhao, Drott et al. 1997, FitzGerald, Lacour et al. 2009). Microchannel caliber is an important consideration to promote axon regeneration, device selectivity, and amplification of microchannel potentials. Very small microchannels, as small as 5 μm, have been demonstrated *in vitro* to optimally amplify axon potentials(Wieringa, Wiertz et al. 2010). However, there is a balance between small caliber microchannels to amplify signals and improve selectivity and larger caliber microchannels, which promote and support regeneration. *In vitro* experiments disagree regarding optimal microchannel caliber with Lacour et al demonstrating improved axon ingrowth into wider channels (>30 μm) while Wieringa et al found that entering axons are more likely to turn around within larger channels (20 μm) while smaller channels (10 μm) maintain axon trajectory through the device (Lacour, Atta et al. 2008, Wieringa, Wiertz et al. 2010). Based on the results of *in vivo* experiments, we suggest that smaller microchannels may inhibit axon regeneration due to fasciculation of regenerating axons and the formation of mini-fascicles within microchannels characterized by a fibrous tissue layer that develops along the microchannel wall. Fitzgerald et al histologically characterized this tissue, an average of 25 μm thick, and concluded that microchannels smaller than 50 μm in diameter may not have adequate space for regenerating axons(FitzGerald, Lago et al. 2012). In our laboratory the results of *in vitro* and *in vivo* studies of various regenerative microchannel designs are consistent with the findings of Lacour et al and Fitzgerald et al. We suggest that regeneration is optimized with microchannel diameters in the range of 75 to 150 μm (FitzGerald, Lacour et al. 2009, Srinivasan, Guo et al. 2011, FitzGerald, Lago et al. 2012, Srinivasan, Tahilramani et al. in press). Thus channel diameters of 75 μm and 200 μm (for imbedding a 75 μm microwire) were chosen for these experiments. Axons surrounded by Schwann cells are found in histological sections through microchannels of both sizes suggesting that axon elongation and Schwann cell migration are promoted in both 200 and 75 micrometer diameter microchannels. In addition, there is a peripheral band of tissue surrounding each microchannel similar in appearance to the micro-fascicular architecture and fibrous tissue layer described previously *in vivo* (Tansey, Seifert et al. 2011, FitzGerald, Lago et al. 2012, Srinivasan, Tahilramani et al. in press). Such architecture mimics the compartmentalization of axons transiting peripheral nerve fascicles in an intact nerve in contrast to the large central cords observed after regeneration through single open lumen or thin film nerve conduits (Clements, Kim et al. 2009, Garde, Keefer et al. 2009). This perineurium-like tissue layer may be beneficial by further amplifying and insulating potentials originating from axons within the microchannel. Alternatively, if this tissue layer is not beneficial, novel methods for minimizing the thickness of this layer *in vivo* could promote regeneration into smaller microchannels to further isolate and amplify axon potentials. Additional study is required to further characterize the functional significance of this regenerated tissue layer within microchannels.

In addition to microchannel caliber, device transparency or the surface area open for regeneration is important to promote axon regeneration and restoration of distal functional connections. Initial *in vitro* experiments demonstrate optimal axon ingrowth into microchannel constructs with 50% transparency(Lacour, Atta et al. 2008). *In vivo*, increasing device transparency is associated with an increase in distal axon counts(Lago, Ceballos et al. 2005, Ramachandran, Schuettler et al. 2006, FitzGerald, Lago et al. 2012). The PDMS scaffold presented here has a transparency of 46% available for regeneration. By comparison, the sieve electrodes used by Lago et al and Ramachandran et al included an open surface available for axon regeneration of 11% and 28%, respectively. This increase in transparency, by increasing the number of sieve holes, almost doubled the number of distal axons increasing from 4940 axons to 8441axons after 2 months of regeneration(Lago, Ceballos et al. 2005, Ramachandran, Schuettler et al. 2006). Similarly, Fitzgerald et al reported on two scaffold designs with different transparencies, 21% and 62%, after 3 months of regeneration and noted an increase in the distal axon count with increased transparency(FitzGerald, Lago et al. 2012). However these reports do not account for branching of regenerating axons, likely accounting for reports of distal axon counts after 7 months of regeneration exceeding counts in the native nerve(Ramachandran, Schuettler et al. 2006). Similarly, axon branching can influence distal target EMG recordings since branching axons can establish multiple connections with distal muscle targets and increase direct motor responses to nerve stimulation. Essentially both distal axon counts and electrophysiology methods have the same limitation in quantifying regeneration. Although systematic evaluation of axons in the distal nerve were not performed in this experiment, the restoration of distal muscle responses reported here is a correlate for distal axon regeneration. The restoration of distal muscle responses reported here is likely influenced by the relatively high device transparency, consistent with previous in vivo reports. This further supports the notion that minimizing obstruction to regeneration by increasing transparency is a critical design consideration for peripheral neural interfaces.

During explant of the regenerated sciatic nerve and device in euthanized animals, no evidence of a neuroma was seen surrounding the external suture guide, suggesting that axons regenerated into microchannels as intended. This is consistent with other regenerative electrode designs which include a suture guide encasing the sieve or microchannel scaffold and in which axons regenerate through the device and were permitted to reach distal targets (Lago, Ceballos et al. 2005, Ramachandran, Schuettler et al. 2006, Lago and Navarro 2007, FitzGerald, Lago et al. 2012). Of note in Figure 4(A), the bright field image shows a thin rim of tissue surrounding the PDMS scaffold, the space between the PDMS scaffold and the surrounding suture guide. The presence of this space is a limitation for microchannel scaffold designs implanted with a suture guide or insert tube and a similar space is also noted in rolled microchannel scaffolds within the open central core created by rolling(FitzGerald, Lago et al. 2012, Stoyanova, van Wezel et al. 2013, Srinivasan, Tahilramani et al. in press). Such open spaces result in a relative increase in device transparency, allowing axons to regenerate across the scaffold without regenerating into sieve holes or microchannels. The contribution of axon regeneration through such spaces to distal axon counts and functional recovery is likely relative to the device transparency created by open microchannels. Some designs occlude such spaces while others report that

the relative contribution to the transparency of the device is minimal and the space remains open(FitzGerald, Lago et al. 2012, Srinivasan, Tahilramani et al. in press). Stoyanova et al developed a novel microchannel scaffold design with bifurcating microchannels, which has a rectangular shape when fabricated and is implanted within an insert tube. Axon regeneration in the space between the rectangular scaffold and the insert tube was quantified and accounted for two-thirds of axons in the distal nerve(Stoyanova, van Wezel et al. 2013). The relative increase in transparency created by the scaffold/tube shape mismatch may account for the volume of axons regenerating in this space since the scaffold transparency, assuming a 1.5mm inner tube diameter, is only 12% based on microchannels alone. In our design with high device transparency from microchannels, the small space between the scaffold and the suture guide is likely of little consequence. In contrast, designs with few scaffold microchannels and low transparency may expect to see more regeneration through such spaces especially if there is a mismatch between the scaffold shape and the suture guide, as is the case for Stoyanova et al. In the present report axons regenerating within the space around the scaffold were not quantified. In the horizontal section of the distal nerve in Figure 4(B), a thin ribbon of tissue, immunoreactive for NF-160, is noted exiting this space and joining the distal nerve. In this image these axons appear to account for a remarkably small proportion of axons exiting microchannels and although it is possible that a few of these axons may have regenerated distally, they are unlikely to account for the magnitude of our reported results. Nevertheless, based on these findings we recommend improving the adhesion between the microchannel scaffold and the suture guide to eliminate this space in future designs.

Restoration of spinal reflexes, as assessed by H reflex recovery, also occurred in a similar time frame in Microchannel and Control groups. Previous studies have reported recovery of spinal reflexes across open lumen synthetic nerve grafts but compared with direct end-to-end repair, recovery was delayed (Valero-Cabre and Navarro 2001). The results of these studies are difficult to compare directly to our findings because synthetic nerve grafts are designed to bridge nerve gaps, requiring regeneration across synthetic conduits often greater than10 mm in length, longer than the 3mm PDMS scaffold used here, which was designed specifically for peripheral neural interfacing (Valero-Cabre and Navarro 2001, Kim, Haftel et al. 2008). The average latency from stimulation to the direct muscle response decreased over time in Microchannel and Control groups, returning to intact, pre-transection values by 80 days in both groups. The latency from stimulation to response is a function of a restoration of the intrinsic properties of the motoneurons as well as myelination of the regenerated axons, mediated by Schwann cells (Foehring, Sypert et al. 1986). In histological sections through microchannel interfaces explanted as early as 32 days post transection, profiles of axons surrounded by Schwann cells are visible within microchannels, indicating the presence of nearby Schwann cells capable of myelinating axons. Although we cannot be certain that these myelinated axons within the microchannels are regenerating motor axons, if combined with our electrophysiological evidence of functional motor reinnervation, it is likely that at least some of them are axons of motoneurons.

4.3 Discrete potentials recorded from within microchannels in awake and behaving animals

In these preliminary experiments, stimulation evoked and volitional locomotion recordings were made from microchannels in a small group of awake and behaving animals. As previously discussed, stimulation evoked microchannel potentials are likely recorded from a combination of sensory and motor axons. Potentials with unique stimulation thresholds, latencies, and waveforms were found in different microchannels in the same animal, likely resulting from different types of regenerated axons. These potentials were unique across microchannels, illustrated in Figure 5(C), and included responses which were likely from both single and multi-axon potentials. Raster plots of waveforms recorded from microchannels simultaneously during ramped stimulation suggest recruitment of unique microchannel potentials with increasing stimulus intensity. The evoked potentials recorded in these experiments have amplitudes and waveforms consistent with other *in vitro* and *in vivo* microchannel potential recordings (FitzGerald, Lacour et al. 2009, FitzGerald, Lago et al. 2012, Minev, Chew et al. 2012). Based on these results, we suggest that these evoked potentials are recordings of single or multiple axons regenerated within microchannels.

It is important to note that these microchannel recordings were recorded amid EMG activity generated in adjacent muscles, which are active in awake and behaving animals. This is in contrast to experimental procedures using anesthetized animals in which muscle activity is quieted. As previously discussed, potentials recorded within microchannels are amplified, insulated, and independent of electrode position, resulting in enhanced recording of small potentials(FitzGerald, Lacour et al. 2009). In the present results, microchannel potential recordings were obtained at sub-maximal stimulation levels, in the absence of TA activation, illustrated in Figure 5. These experiments were conducted to progressively stimulate uncut axons in the proximal nerve in an attempt to isolate small populations of regenerated microchannel axons with the lowest thresholds for firing, typically the largest axons.

Although we cannot be certain that other muscles not instrumented during the experiments may have contaminated these microchannel responses, we believe that these findings represent the activation of motor axons, amplified by microchannels in behaving animals, based on four primary observations. First, microchannel recordings were made with band pass filters in place that selected for a frequency range of 1-10 kHz. This was a conscious effort to limit the contributions of EMG potentials to our microchannel recordings. The peak power spectrum of EMG potentials would be expected to be in the 100-500 Hz range and thus their contributions to our microchannel recordings would be expected to be attenuated significantly by our filtering strategy(Basmajian and DeLuca 1985). Second, responses were unique to the microchannel sampled, with different potentials recorded from different microchannels during simultaneous stimulation. This is illustrated by the microchannel raster plots in Figure 5(C). We would expect a signal originating outside of the neural interface, such as from muscle contamination, to occur in multiple microchannels simultaneously. Third, the simultaneous TA muscle recordings have baseline noise amplitude which is greater than the amplitude of potentials recorded within the microchannels. This suggests that microchannels are amplifying small potentials within the high extracellular resistance environment of the microchannel space, consistent with the

findings of Fitzgerald et al (FitzGerald, Lacour et al. 2009). We would not expect microchannels to amplify lower frequency muscle potentials originating outside of the insulated microchannel. Finally, the response waveforms were consistent with other reports of stimulation-evoked recordings within microchannels, typically triphasic responses (FitzGerald, Lacour et al. 2009, FitzGerald, Lago et al. 2012, Minev, Chew et al. 2012). Polyphasic waveforms, such as the microchannel 2 response in Figure 5(C), could represent reinnervated muscle contamination but given the response is only present in a single microchannel and the amplitude is smaller than the TA EMG background activity, the more likely explanation is that we are recording from a small population of axons within the microchannel.

4.3 Volitional, efferent motor potentials recorded from within microchannels during locomotion

Microchannel potentials were also recorded during treadmill locomotion and, when the timing of extracted action potentials is correlated with muscle activity, we identified these potentials as containing the discharge of active motor axons. The contribution of motor axon potentials to the microchannel potentials represent volitional efferent activity generated centrally during animal locomotion. There are no prior reports of microchannel recordings and few reports of reinnervated peripheral nerve recordings in awake and behaving rats for direct comparison with our preliminary results. Garde et al recorded peripheral nerve potentials from the regenerated sciatic nerve in awake animals through a single lumen open conduit regenerative interface (Garde, Keefer et al. 2009). These relatively large amplitude potentials, ranging from 300-1000 μV, were likely recorded from either very large regenerated axons or perhaps from passive conduction of nearby muscle activity. By comparison, sieve electrodes and *in vivo* microchannel evoked potentials recorded from the peripheral nerve in anesthetized animals are generally reported in the 50-200 μV range, consistent with the amplitudes of microchannel potentials recorded here (Mensinger, Anderson et al. 2000, Ramachandran, Schuettler et al. 2006, FitzGerald, Lago et al. 2012).

Microchannel potentials extracted during locomotion were further characterized with step cycle analysis and the firing of these potentials was consistent with patterns previously described after sciatic nerve regeneration. The probability of firing during multiple step cycles, illustrated in Figure 6, suggest that many of these motor axons begin firing in the middle of the swing phase of locomotion and maintain firing through most of the step cycle. In intact animals, such a firing pattern would be more closely associated with motor axons innervating ankle extensor muscles, such as SOL, than with flexor muscles such as TA. However, after sciatic nerve transection and successful axon regeneration, we have previously demonstrated that TA and SOL are co-activated during locomotion with activity in TA especially prolonged to include both swing and stance phases of gait (English, Chen et al. 2007). Similar flexor and extensor locomotion activation patterns have also been demonstrated following cervical cord (C7) hemisection in rats, suggesting central reorganization of locomotor pattern activation following injury (Dominici, Keller et al. 2012). The dominant pattern of activation in extracted motor axon potentials during these locomotion experiments is consistent with these previous observations.

In locomotion experiments, motor potentials have been recorded in intact rats from *muscle* using micro-EMG (Gorassini, Eken et al. 2000). These motor potentials are recorded by microelectrodes implanted in close proximity to the motor unit end-plate and are amplified by the muscle. These studies observed firing profile variability in TA similar to patterns recorded here from motor axons regenerated within microchannels. The firing of these motor axons during locomotion, including step cycle activation patterns, is likely influenced by both the intrinsic properties of the motor unit and synaptic inputs from locomotor networks at the level of the spinal cord. Whether these observed firing patterns in these preliminary results represent the reinnervation of the TA muscle by extensor motoneurons whose axons have been misdirected during regeneration, as we have speculated previously, and/or a novel pattern of activation that underlies changes in locomotor networks, must await the results of future studies.

5. Conclusions

We have identified the regeneration of motor axons through a microchannel neural interface and demonstrated the recording of regenerated motor axons within microchannels in awake and behaving animals. With these unique findings, we provide preliminary evidence that the microchannel based peripheral neural interface can be used to record volitional, efferent motor potentials. Such functionality is a critical requirement for any neural interface intended to facilitate direct neural control of external technologies.

Acknowledgments

We would like to thank Jennifer Nicolini and Sohee Park for technical laboratory assistance. This work was supported by NIH/NINDS R25 (RKG) and NS065109 (RVB).

References

Akin T, Najafi K, Smoke RH, Bradley RM. A micromachined silicon sieve electrode for nerve regeneration applications. IEEE Trans Biomed Eng. 1994; 41(4):305–313. [PubMed: 8063296]

Badia J, Boretius T, Andreu D, Azevedo-Coste C, Stieglitz T, Navarro X. Comparative analysis of transverse intrafascicular multichannel, longitudinal intrafascicular and multipolar cuff electrodes for the selective stimulation of nerve fascicles. Journal of Neural Engineering. 2011; 8(3)

Basmajian, JV.; DeLuca, CJ. Muscles alive: their functions revealed by electromyography. Baltimore, MD: Williams & Wilkins; 1985.

Boeltz T, Ireland M, Mathis K, Nicolini J, Poplavski K, Rose SJ, Wilson E, English AW. Effects of treadmill training on functional recovery following peripheral nerve injury in rats. J Neurophysiol. 2013; 109(11):2645–2657. [PubMed: 23468390]

Branner A, Stein RB, Fernandez E, Aoyagi Y, Normann RA. Long-term stimulation and recording with a penetrating microelectrode array in cat sciatic nerve. IEEE Trans Biomed Eng. 2004; 51(1): 146–157. [PubMed: 14723504]

Castro J, Negredo P, Avendano C. Fiber composition of the rat sciatic nerve and its modification during regeneration through a sieve electrode. Brain Res. 2008; 1190:65–77. [PubMed: 18086465]

Ceballos D, Valero-Cabre A, Valderrama E, Schuttler M, Stieglitz T, Navarro X. Morphologic and functional evaluation of peripheral nerve fibers regenerated through polyimide sieve electrodes over long-term implantation. J Biomed Mater Res. 2002; 60(4):517–528. [PubMed: 11948510]

Chen XY, Wolpaw JR. Operant conditioning of H-reflex in freely moving rats. J Neurophysiol. 1995; 73(1):411–415. [PubMed: 7714584]

Clements IP, Kim YT, English AW, Lu X, Chung A, Bellamkonda RV. Thin-film enhanced nerve guidance channels for peripheral nerve repair. Biomaterials. 2009; 30(23-24):3834–3846. [PubMed: 19446873]

Clements IP, Mukhatyar VJ, Srinivasan A, Bentley JT, Andreasen DS, Bellamkonda RV. Regenerative scaffold electrodes for peripheral nerve interfacing. IEEE Trans Neural Syst Rehabil Eng. 2013; 21(4):554–566. [PubMed: 23033438]

Dhillon GS, Lawrence SM, Hutchinson DT, Horch KW. Residual function in peripheral nerve stumps of amputees: implications for neural control of artificial limbs. The Journal of Hand Surgery. 2004; 29(4):605–615. [PubMed: 15249083]

Dominici N, Keller U, Vallery H, Friedli L, van den Brand R, Starkey ML, Musienko P, Riener R, Courtine G. Versatile robotic interface to evaluate, enable and train locomotion and balance after neuromotor disorders. Nat Med. 2012; 18(7):1142–1147. [PubMed: 22653117]

Edell DJ. A peripheral nerve information transducer for amputees: long-term multichannel recordings from rabbit peripheral nerves. IEEE Trans Biomed Eng. 1986; 33(2):203–214. [PubMed: 3007332]

English AW. Enhancing axon regeneration in peripheral nerves also increases functionally inappropriate reinnervation of targets. J Comp Neurol. 2005; 490(4):427–441. [PubMed: 16127712]

English AW, Chen Y, Carp JS, Wolpaw JR, Chen XY. Recovery of electromyographic activity after transection and surgical repair of the rat sciatic nerve. Journal of Neurophysiology. 2007; 97(2): 1127–1134. [PubMed: 17122310]

FitzGerald JJ, Lacour SP, McMahon SB, Fawcett JW. Microchannel Electrodes for Recording and Stimulation: In Vitro Evaluation. Ieee Transactions on Biomedical Engineering. 2009; 56(5): 1524–1534. [PubMed: 19203882]

FitzGerald JJ, Lago N, Benmerah S, Serra J, Watling CP, Cameron RE, Tarte E, Lacour SP, McMahon SB, Fawcett JW. A regenerative microchannel neural interface for recording from and stimulating peripheral axons in vivo. J Neural Eng. 2012; 9(1):016010. [PubMed: 22258138]

Foehring RC, Sypert GW, Munson JB. Properties of self-reinnervated motor units of medial gastrocnemius of cat. II. Axotomized motoneurons and time course of recovery. J Neurophysiol. 1986; 55(5):947–965. [PubMed: 3711974]

Garde K, Keefer E, Botterman B, Galvan P, Romero MI. Early interfaced neural activity from chronic amputated nerves. Front Neuroeng. 2009; 2:5. [PubMed: 19506704]

Gorassini M, Eken T, Bennett DJ, Kiehn O, Hultborn H. Activity of hindlimb motor units during locomotion in the conscious rat. J Neurophysiol. 2000; 83(4):2002–2011. [PubMed: 10758110]

Hariz MI. Complications of deep brain stimulation surgery. Mov Disord. 2002; 17 Suppl 3:S162–166. [PubMed: 11948772]

Kim YT, Haftel VK, Kumar S, Bellamkonda RV. The role of aligned polymer fiber-based constructs in the bridging of long peripheral nerve gaps. Biomaterials. 2008; 29(21):3117–3127. [PubMed: 18448163]

Klinge PM, Vafa MA, Brinker T, Brandis A, Walter GF, Stieglitz T, Samii M, Wewetzer K. Immunohistochemical characterization of axonal sprouting and reactive tissue changes after long-term implantation of a polyimide sieve electrode to the transected adult rat sciatic nerve. Biomaterials. 2001; 22(17):2333–2343. [PubMed: 11511030]

Lacour SP, Atta R, FitzGerald JJ, Blamire M, Tarte E, Fawcett J. Polyimide micro-channel arrays for peripheral nerve regenerative implants. Sensors and Actuators A: Physical. 2008; 147(2):456–463.

Lacour SP, Benmerah S, Tarte E, FitzGerald J, Serra J, McMahon S, Fawcett J, Graudejus O, Yu Z, Morrison B 3rd. Flexible and stretchable micro-electrodes for in vitro and in vivo neural interfaces. Med Biol Eng Comput. 2010; 48(10):945–954. [PubMed: 20535574]

Lago N, Ceballos D, Rodriguez FJ, Stieglitz T, Navarro X. Long term assessment of axonal regeneration through polyimide regenerative electrodes to interface the peripheral nerve. Biomaterials. 2005; 26(14):2021–2031. [PubMed: 15576176]

Lago N, Navarro X. Evaluation of the long-term regenerative potential in an experimental nerve amputee model. Journal of the Peripheral Nervous System. 2007; 12(2):108–120. [PubMed: 17565536]

Mannard A, Stein RB, Charles D. Regeneration electrode units: implants for recording from single peripheral nerve fibers in freely moving animals. Science. 1974; 183(4124):547–549. [PubMed: 4809567]

Mensinger AF, Anderson DJ, Buchko CJ, Johnson MA, Martin DC, Tresco PA, Silver RB, Highstein SM. Chronic recording of regenerating VIIIth nerve axons with a sieve electrode. J Neurophysiol. 2000; 83(1):611–615. [PubMed: 10634898]

Minev IR, Chew DJ, Delivopoulos E, Fawcett JW, Lacour SP. High sensitivity recording of afferent nerve activity using ultra-compliant microchannel electrodes: an acute in vivo validation. J Neural Eng. 2012; 9(2):026005. [PubMed: 22328617]

Navarro X, Calvet S, Rodriguez FJ, Stieglitz T, Blau C, Buti M, Valderrama E, Meyer JU. Stimulation and recording from regenerated peripheral nerves through polyimide sieve electrodes. J Peripher Nerv Syst. 1998; 3(2):91–101. [PubMed: 10959242]

Polikov VS, Tresco PA, Reichert WM. Response of brain tissue to chronically implanted neural electrodes. Journal of Neuroscience Methods. 2005; 148(1):1–18. [PubMed: 16198003]

Ramachandran A, Schuettler M, Lago N, Doerge T, Koch KP, Navarro X, Hoffmann KP, Stieglitz T. Design, in vitro and in vivo assessment of a multi-channel sieve electrode with integrated multiplexer. J Neural Eng. 2006; 3(2):114–124. [PubMed: 16705267]

Rutten WL. Selective electrical interfaces with the nervous system. Annu Rev Biomed Eng. 2002; 4:407–452. [PubMed: 12117764]

Sabatier MJ, Bao NT, Nicolini J, English AW. Effect of Axon Misdirection on Recovery of Electromyographic Activity and Kinematics after Peripheral Nerve Injury. Cells Tissues Organs. 2011; 193(5):298–309. [PubMed: 21411964]

Sabatier MJ, Redmon N, Schwartz G, English AW. Treadmill training promotes axon regeneration in injured peripheral nerves. Exp Neurol. 2008; 211(2):489–493. [PubMed: 18420199]

Serra J, Bostock H, Navarro X. Microneurography in rats: a minimally invasive method to record single C-fiber action potentials from peripheral nerves in vivo. Neurosci Lett. 2010; 470(3):168–174. [PubMed: 19800936]

Srinivasan A, Guo L, Bellamkonda RV. Regenerative microchannel electrode array for peripheral nerve interfacing. IEEE. 2011

Srinivasan A, Tahilramani M, Bentley JT, Gore KK, Millard D, Mukhatyar VJ, Joseph A, Haque A, Stanley GB, English AW, Bellamkonda RV. Microchannel-based Regenerative Scaffold for Chronic Peripheral Nerve Interfacing in Amputees. Biomaterials. in press.

Stein RB, Nichols TR, Jhamandas J, Davis L, Charles D. Stable long-term recordings from cat peripheral nerves. Brain Research. 1977; 128(1):21–38. [PubMed: 871910]

Stieglitz T. Neural prostheses in clinical practice: biomedical microsystems in neurological rehabilitation. Acta Neurochir Suppl. 2007; 97(Pt 1):411–418. [PubMed: 17691404]

Stieglitz T, Beutel H, Blau C, Meyer JU. Flexible multichannel microelectrodes with integrated leads for use in neuroprosthetics. Biomed Tech (Berl). 1997; 42 Suppl:449–450. [PubMed: 9517231]

Stoyanova II, van Wezel RJ, Rutten WL. In vivo testing of a 3D bifurcating microchannel scaffold inducing separation of regenerating axon bundles in peripheral nerves. J Neural Eng. 2013; 10(6): 066018. [PubMed: 24280623]

Tansey KE, Seifert JL, Botterman B, Delgado MR, Romero MI. Peripheral nerve repair through multi-luminal biosynthetic implants. Ann Biomed Eng. 2011; 39(6):1815–1828. [PubMed: 21347549]

Valero-Cabre A, Navarro X. H reflex restitution and facilitation after different types of peripheral nerve injury and repair. Brain Research. 2001; 919(2):302–312. [PubMed: 11701142]

Wieringa PA, Wiertz RWF, de Weerd EL, Rutten WLC. In vitro Verification of a 3-D Regenerative Neural Interface Design: Examination of Neurite Growth and Electrical Properties Within a Bifurcating Microchannel Structure. Proceedings of the Ieee. 2010; 98(3):389–397.

Zhao Q, Drott J, Laurell T, Wallman L, Lindstrom K, Bjursten LM, Lundborg G, Montelius L, Danielsen N. Rat sciatic nerve regeneration through a micromachined silicon chip. Biomaterials. 1997; 18(1):75–80. [PubMed: 9003901]

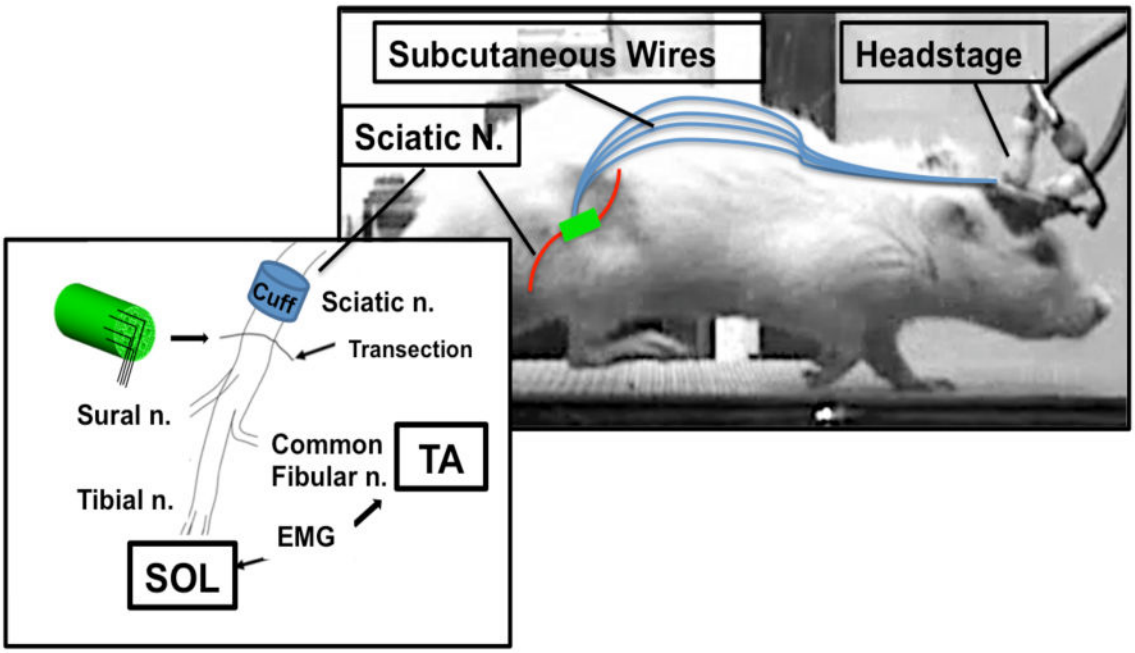

Figure 1.

Schematic representation of experimental setup. All animals were implanted with a stimulating cuff electrode about the sciatic nerve in the mid-thigh and bipolar fine-wire EMG recording electrodes into the tibialis anterior (TA) and soleus (SOL) muscles. After baseline intact electrophysiological recordings were obtained the sciatic nerve was transected distal to the cuff electrode and then repaired either by attaching the proximal and distal cut nerve segments to the ends of a microchannel neural interface (Microchannel group) or by direct end-to-end nerve repair (Control Group). Wires from all implanted hardware were passed subcutaneously from the right hindlimb to a pair of head-mounted connector plugs (Headstage). An exteriorized ground electrode was attached to bone screws used to secure the connector plugs to the animal's skull.

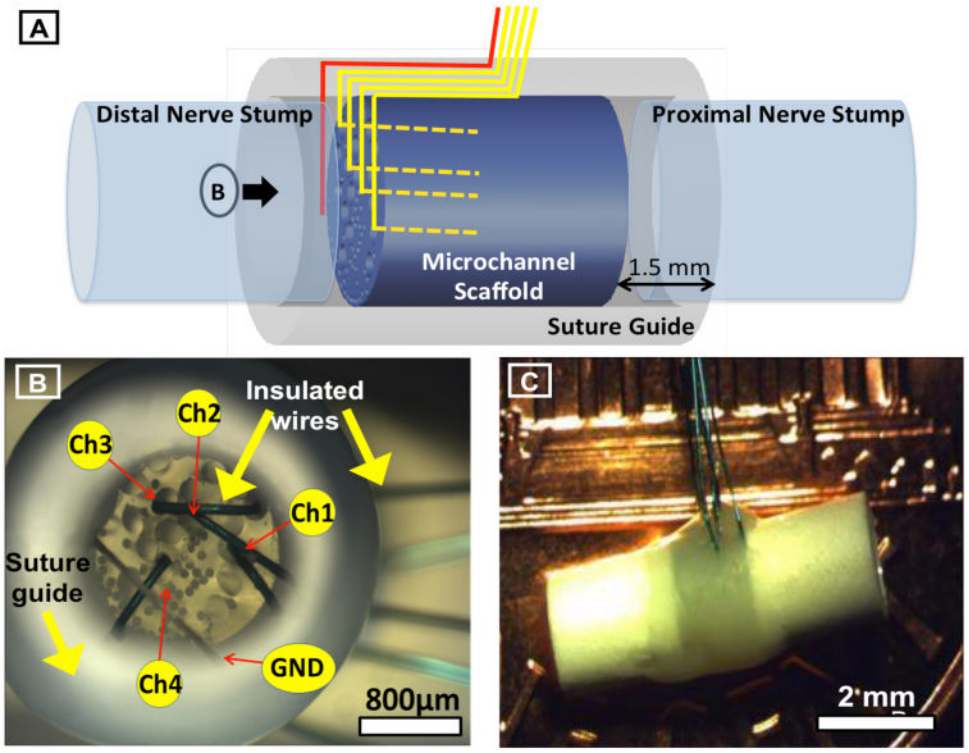

Figure 2.

Details of microchannel neural interface. A. Schematic representation of the peripheral neural interface with customizable PDMS microchannels and integrated microwire electrodes, illustrating the 3mm long PDMS microchannel scaffold (blue), the surrounding polysulfon suture guide (gray), the integrated microwire electrodes transiting between the suture guide and scaffold to the distal end and then entering microchannels (yellow), and the ground wire at the distal end of the device (red). Proximal and distal nerve stumps are shown to illustrate configuration after implantation. B. Microscope photograph view of the distal end of the neural interface prior to implantation (shown by the arrow marked B in panel A). Microchannels of 200 and 75 µm diameters are visible on the distal face of the PDMS scaffold. Microchannels containing microwire electrodes (200µm) are labeled (Ch1-4) as well as the ground wire (GND). Insulated microwires are seen transiting between the microchannel scaffold and the suture guide prior to exiting the device. C. Microscope photograph of the final assembled neural interface prior to implantation illustrating the external polysulfon suture guide and exiting microwires.

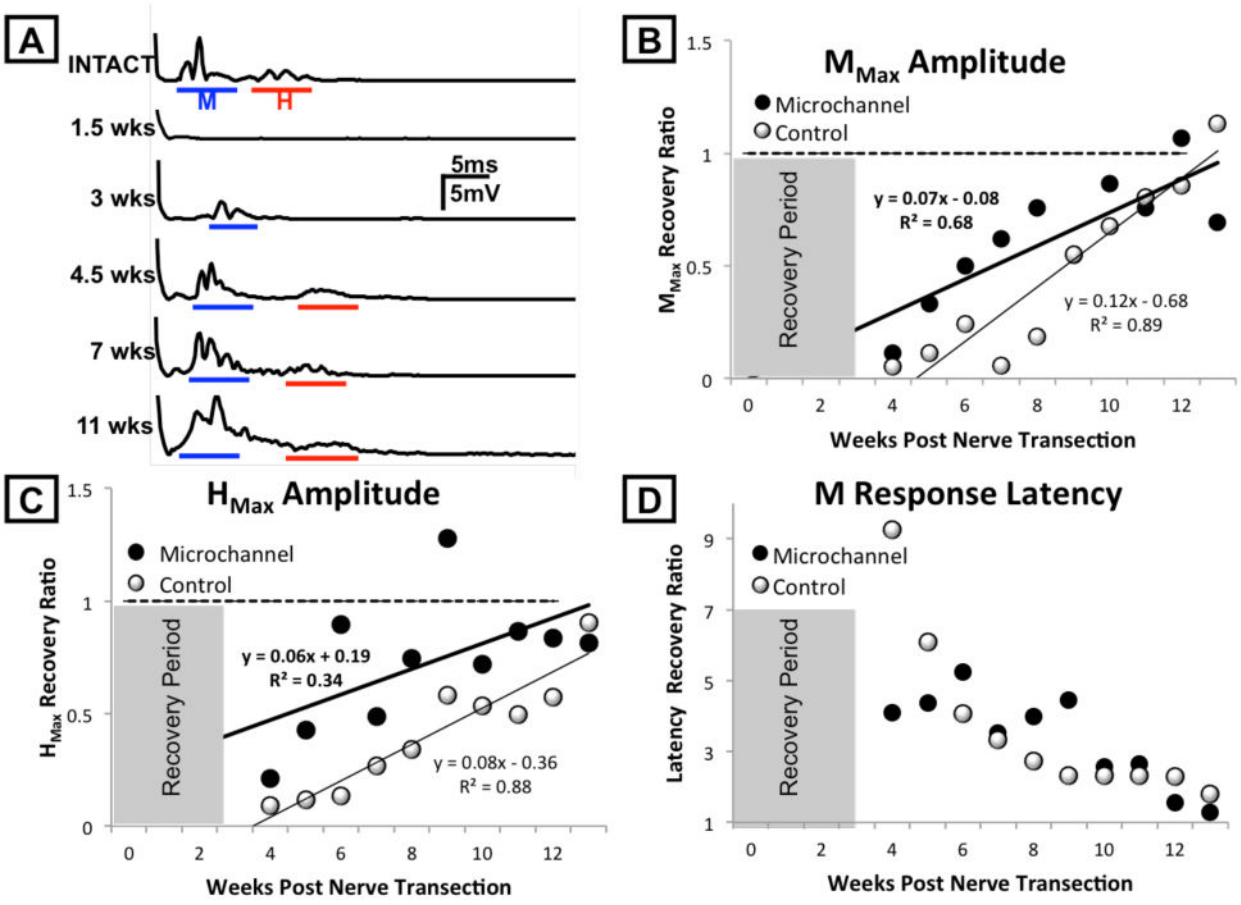

Figure 3.

Regenerating axons elongate through the microchannel neural interface and reinnervate muscle targets. A. Recordings of EMG activity in the soleus muscle of a representative animal in response to stimulation of the sciatic nerve before (top trace) and at different time points after transection of the sciatic nerve and repair using a microchannel neural interface is shown as rectified and average potentials. Recovery of responses at direct muscle (M) response and H reflex latencies are shown as solid lines beneath each trace. B. The maximum evoked voltage recorded in the M response time window in post-transection rats was expressed as a proportion of the same measure in the same rats prior to nerve transection and repair, either using a microchannel neural interface (Microchannel, dark circles) or simple end-to-end nerve repair (Control, white circles), and displayed over the course of the study period. Each symbol is an average of several rats (Control=8, Microchannel =10). The horizontal dashed line at 1.0 indicates the amplitude of full pre-transection restoration of the M response. Data were fit with linear least square regression methods. C. The maximum evoked voltage recorded in the H reflex time window in post-transection rats was expressed as a proportion of the same measure in the same rats prior to nerve transection and repair. Data are displayed as in panel B. D: The mean latencies, from stimulus to initial M response over time after sciatic transection for Microchannel (dark circles) and Control (white circles) rats. Values are expressed as a proportion of the

respective latency recorded prior to nerve transection. Shaded areas in panels B-D indicate the time period for recovery after nerve transection prior to study of evoked potentials.

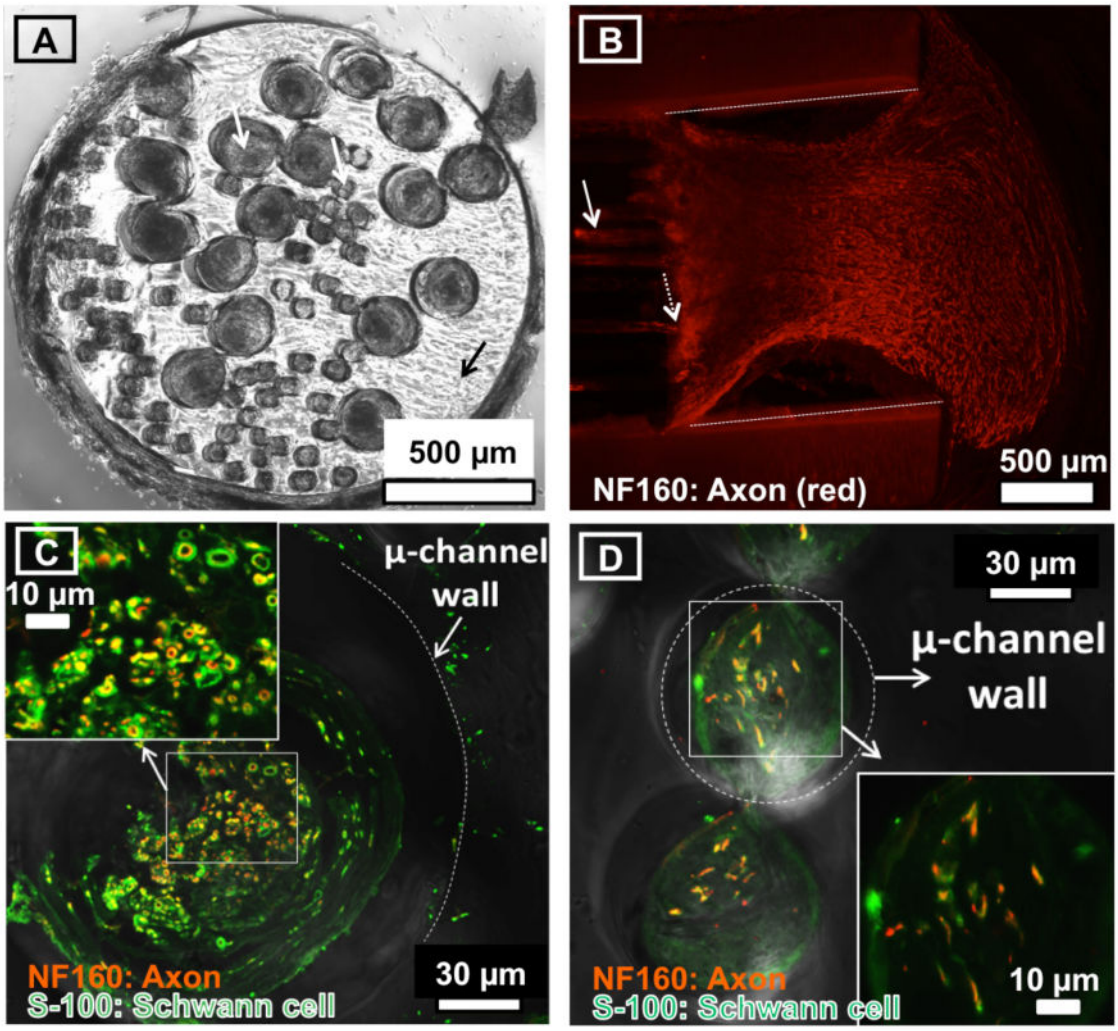

Figure 4.

Tissue containing both Schwann cells and regenerating axons is found in microchannels. A: Bright field image of a transverse histological section through the proximal end of the PDMS microchannel scaffold (black arrow) explanted 32 days after nerve transection and repair. Both the 200 and 75 µm diameter microchannels contain regenerated tissue (white arrows). B: Confocal image of a horizontal section of the distal end of the microchannel neural interface after sciatic nerve transection and repair. Profiles of regenerating axons are marked by immunoreactivity to neurofilament proteins (NF-160, red). The distal end of the PDMS microchannel scaffold contains regenerated axons within microchannels (sold white arrow). Regenerated axons exit the distal microchannels (dashed white arrow) and form a distal nerve seen here within the neural interface suture guide. The suture guide wall is labeled with dashed white lines for reference. C and D: Confocal images of a transverse section of the distal end of the microchannel neural interface 32 days after sciatic nerve transection and repair. In both panels C and D, profiles of regenerating axons are marked by immunoreactivity to neurofilament proteins (NF-160, red) and those of Schwann cells are marked by immunoreactivity to S-100 (green). C. A single 200 µm diameter microchannel contains regenerated axons (red) and Schwann cells (green). Axons surrounded by Schwann

cells are apparent (inset). The PDMS microchannel wall is labeled with a white dotted line for reference. D: Two adjacent 75 μm diameter microchannels contain regenerated axons (red) and schwann cells (green). Axons surrounded by Schwann cells are apparent (inset). A PDMS microchannel wall is labeled with a dashed white dotted line for reference.

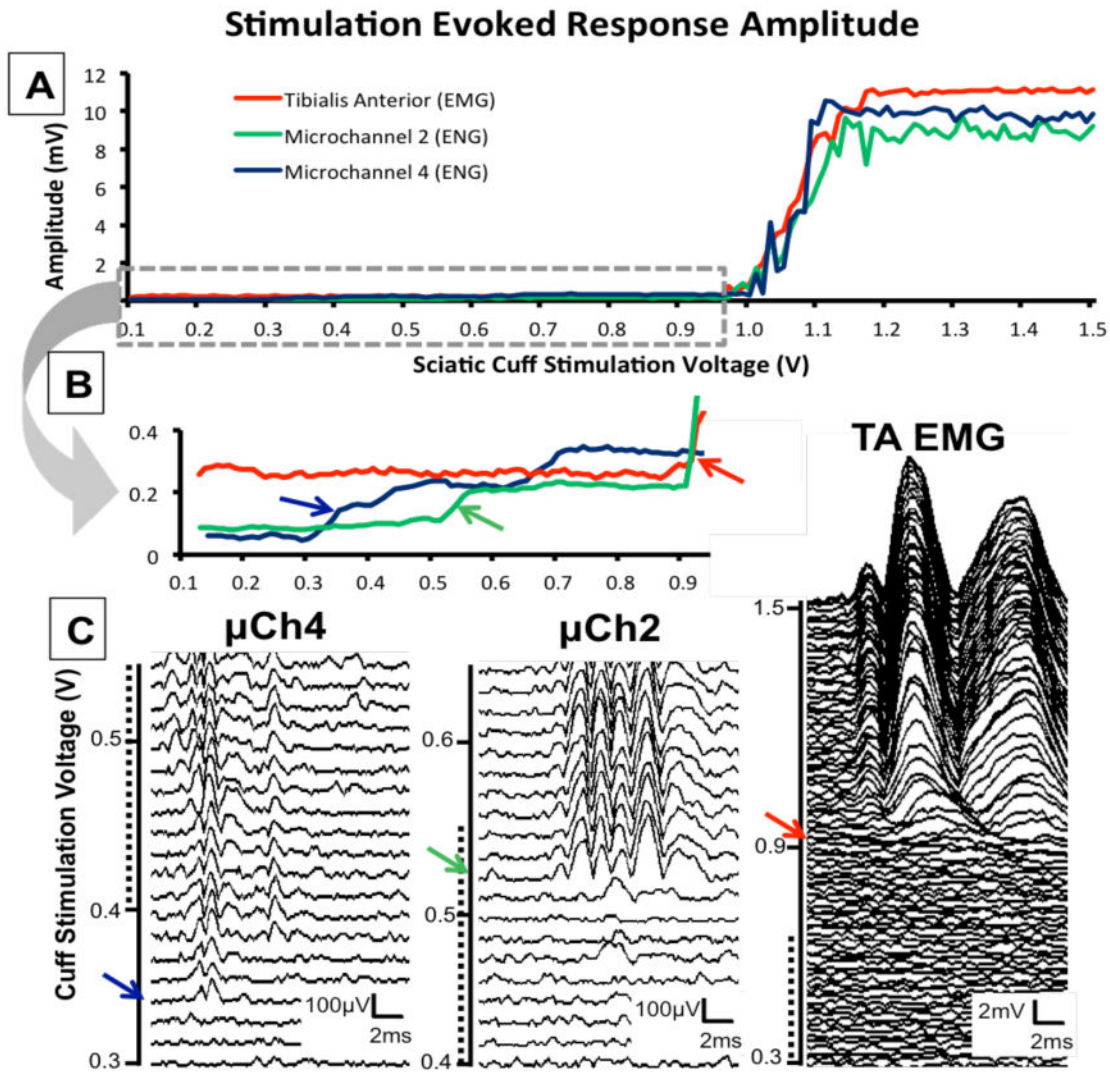

Figure 5.

Responses recorded in two microchannels and the reinnervated TA muscle during stimulation of the sciatic nerve at progressively increasing intensities in an awake and behaving rat 54 days after sciatic transection and repair across a microchannel neural interface. Very short (0.1 ms) monophasic constant voltage pulses were delivered to the sciatic nerve through the implanted sciatic cuff starting at sub-maximal (0.15 V) stimulation and successively increasing stimulus voltage up to supra-maximal stimulation (1.5 V). Recordings were made during ∼120 successive stimulations with at least a 3 s inter-stimulus delay. A. The peak-to-peak amplitude of TA (red), microchannel 2 (green), and microchannel 4 (blue) responses during ramped stimulation of the sciatic nerve. B: Traces in panel A are expanded to include only sub-maximal stimulation intensities (0.15 – 1.0 V). C: Potentials from progressively increasing cuff stimulation are displayed in raster plots including ∼20 sweeps for microchannel potentials and ∼100 sweeps for TA EMG potentials. Dotted lines correspond to overlapping stimulation voltages for each raster. Color arrows (red, green and blue) on each amplitude trace in B correspond to recorded potentials

in C with unique waveforms recorded simultaneously in microchannels. Waveforms are the direct response to a single stimulation at the specified intensity.

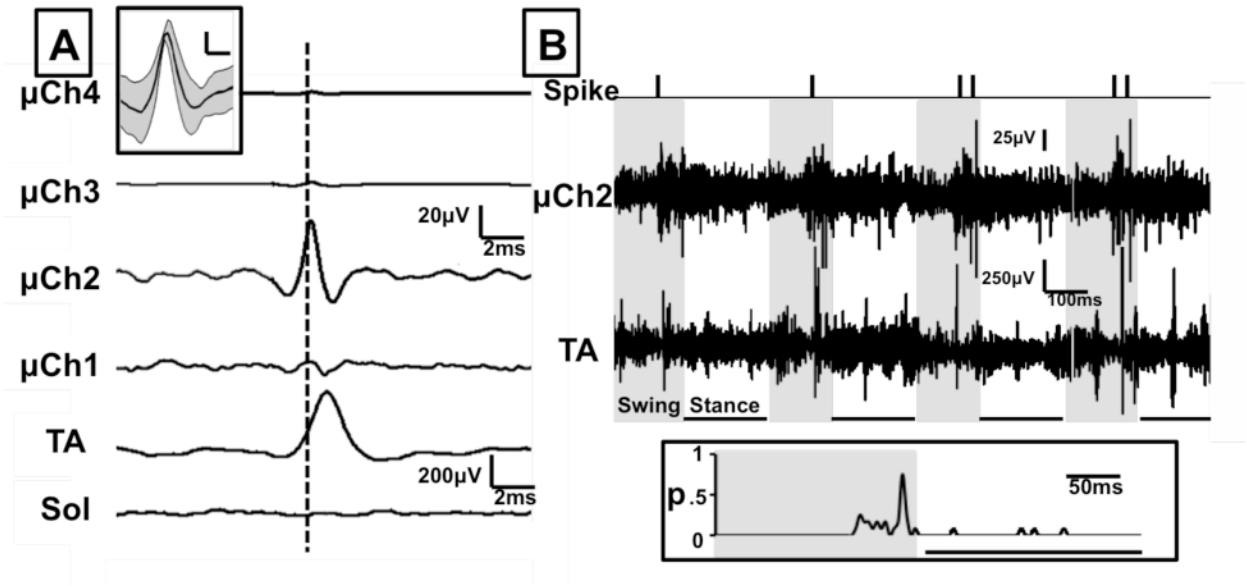

Figure 6.

Single unit action potentials could be discriminated and extracted from the potentials recorded from microwires in the microchannels. Action potentials with similar waveforms were identified in the microchannel recordings obtained during treadmill locomotion and extracted using a time-amplitude window discriminator routine. A. The timing of these potentials was used to characterize single unit potentials with spike triggered averaging. Time locked average responses to the firing of one unit (vertical dashed line), recorded 51 days after sciatic transection, are shown for tibialis anterior (TA) and Soleus (Sol) EMG activity, and all four microchannels (μCh1-4). Inset: Average (dark line) action potential and variance in waveform shape about this average (shaded area) for this TA motor unit. Scale bar = 10μV/1ms. B. The timing of activity of this single unit (Spike), microchannel 2 activity (μCh2), and tibialis anterior EMG activity (TA) are displayed for four consecutive step cycles while walking on a level treadmill. Activity was synchronized with video recordings of treadmill locomotion. Shaded time periods represent the swing phase and underlined time periods represent the stance phase of the step cycle. Inset: probability of firing of this TA motor unit during a step cycle, as determined from spike timing during 12 consecutive steps.